

Structural, Spectroscopic, and Magnetic Study of Bis(9,10-dihydro-9-oxo-10-acridineacetate)bis(imidazole)bis(methanol) Nickel(II)

Danuta Dobrzyńska,^{*,†} Lucjan B. Jerzykiewicz,[‡] Marek Duczmal,[†] Agnieszka Wojciechowska,[†] Katarzyna Jabłońska,[†] Jerzy Palus,[†] and Andrzej Ożarowski[§]

Faculty of Chemistry, Wrocław University of Technology, Wybrzeże Wyspiańskiego 27, 50-370 Wrocław, Poland, Faculty of Chemistry, University of Wrocław, Joliot-Curie 14, 50-383 Wrocław, Poland, and National High Magnetic Field Laboratory, Florida State University, 1800 East Paul Dirac Drive, Tallahassee, Florida 32310

Received May 22, 2006

The mixed ligand complex $[\text{Ni}(\text{CMA})_2(\text{im})_2(\text{MeOH})_2]$ (where CMA = 9,10-dihydro-9-oxo-10-acridineacetate ion, im = imidazole) was prepared, and its crystal and molecular structure were determined. The nickel ions are hexa-coordinated by four oxygen atoms of the carboxylate and hydroxyl groups and by two imidazole nitrogen atoms, to form a distorted octahedral arrangement. The structure consists of a one-dimensional network of the complex molecules connected by strong intermolecular hydrogen bonds. The weak intermolecular C–H \cdots X hydrogen bonds and stacking interactions make up the 2-D structure. Very strong intramolecular hydrogen bonds significantly affect the geometry and vibrational characteristics of the carboxylate group. The UV–vis–NIR electronic spectrum was deconvoluted into Gaussian components. Electronic bands of the Ni(II) ion were assigned to suitable spin-allowed transitions in the D_{4h} symmetry environment. The single ion zero-field splitting (ZFS) parameters for the $S = 1$ state of Ni(II), as well as the g components, have been determined by high-field and high-frequency EPR (HF-HFEPR) spectroscopy over the frequency range of 52–432 GHz and with the magnetic fields up to 14.5 T: $D = 5.77(1) \text{ cm}^{-1}$, $E = 1.636(2) \text{ cm}^{-1}$, $g_x = 2.29(1)$, $g_y = 2.18(1)$, and $g_z = 2.13(1)$. These values allowed us to simulate the powder magnetic susceptibility and field-dependent magnetization of the complex.

1. Introduction

The structure of nickel-containing biological sites and their catalytic functions have been studied by many investigators.¹ To date, six distinct classes of nickel-containing enzymes have been identified: the polynuclear hydrogenases, methyl-CoM-reductases, acetyl-CoA-synthases, CO dehydrogenases, the dinuclear enzyme–urease,¹ and mononuclear enzyme superoxide dismutase.² Recently, Davidson and co-workers reported a new type of nickel coordination in the active site of *Escherichia coli* glyoxalase I (GlxI).³ GlxI is involved in the first step of the detoxification of cytotoxic

pyruvaldehyde. The X-ray absorption spectroscopy studies revealed that the nickel center of this enzyme consists of a Ni(II) ion that is hexa-coordinated by two carboxylates, two histidine imidazoles, and two water molecules. Structures of the *E. coli* Glyoxalase I apoenzyme and of the complexes with Ni^{2+} , Co^{2+} , Cd^{2+} , and Zn^{2+} were also determined by X-ray diffraction. It was found that the complexes that are catalytically active have an octahedral geometry (Ni^{2+} , Co^{2+} , and Cd^{2+}). In contrast, the complex of the *E. coli* GlxI enzyme with Zn^{2+} has trigonal bipyramidal coordination (coordination number = 5) and is inactive.⁴ The study of the CD spectra of the apoenzyme and Ni(II)-substituted GlxI in the region 180–250 nm revealed that nickel binding is not essential for dimerization nor for conformation of the

* To whom correspondence should be addressed. E-mail: danuta.dobrzynska@pwr.wroc.pl.

[†] Wrocław University of Technology.

[‡] University of Wrocław.

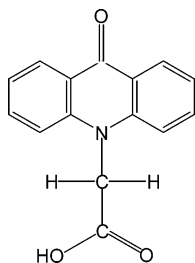
[§] Florida State University.

(1) Cammack, R. *Bioinorganic Catalysis, part 7*; Reedijk, J., Ed.; Marcel Dekker: New York, 1993.

(2) Fiedler, A. T.; Bryngelson, P. A.; Maroney, M. J.; Brunold, T. C. *J. Am. Chem. Soc.* **2005**, *127*, 5449.

(3) Davidson, G.; Clugston, S. L.; Honek, J. F.; Maroney, M. J. *Inorg. Chem.* **2000**, *39*, 2962.

(4) He, M. M.; Cluston, S. L.; Honek, J. F.; Matthews, B. W. *Biochemistry* **2000**, *39*, 8719.

Scheme 1. Molecule of 9,10-Dihydro-9-oxo-10-acridineacetic Acid (CMAH)

protein.⁵ No spectroscopic or magnetic investigations of the paramagnetic center of the *E. coli* Glx1 have been reported as yet. The mononuclear nickel center similar to that of Glx1 was found in the nickel-sensing NmtR repressor from *Mycobacterium tuberculosis*. The nickel ion in this protein is thought to be coordinated to oxygen and nitrogen ligands in a pseudo-octahedron. The UV-vis absorption spectrum confirms such coordination.⁶

The number of reports on monomeric nickel complexes containing the previously mentioned donor set that can be regarded as models of GlxI is quite limited.^{7–11} To mimic the coordination surrounding the Ni(II) ion in GlxI, we have employed biologically important compounds: 9,10-dihydro-9-oxo-10-acridineacetic acid (CMAH), a powerful interferon inducer¹² (Scheme 1), and imidazole. CMAH delivers the carboxylate group for binding Ni(II), whereas imidazole was used to model the histidine residues in the nickel-containing proteins.

Both of the ligands used in our study are interesting from the viewpoint of crystal engineering because they provide covalent coordination bonds, hydrogen bonds of various types, and in the case of CMAH, they also allow extensive π - π interactions. Diverse carboxylate coordination modes have been found in the previously characterized complexes of the CMA⁻ ion with metal ions, Cu(II),^{13,14} Zn(II),¹⁵ Ca(II),¹⁶ and Pb(II),¹⁶ as well as with the D,L-histidinium ion.¹⁷

2. Experimental Procedures

Synthesis. The solution of NiCl₂·6H₂O (0.079 g, 0.33 mmol) in methanol was added to the solution of CMAH¹² (0.169 g, 0.66 mmol) and imidazole (0.114 g, 1.65 mmol) in methanol. After a

few days, green crystals of X-ray quality were deposited, yielding 60.8%. Anal. calcd for NiC₃₈H₃₆N₆O₈: C, 59.79; H, 4.75; N, 11.01%. Found: C, 60.13; H, 4.84; N, 10.78%.

IR (ν /cm⁻¹): 3410(m), 3139(s), 3063(s), 3030(s), 2959(s), 2919(s), 2868(s), 1625(vs), 1595(vs), 1575(vs), 1545(s), 1498(vs), 1462(vs), 1386(vs), 1375(vs), 1331(m), 1291(vs), 1297(vs), 1181(vs), 1135(m), 1095(m), 1067(s), 1045(s), 1003(m), 944(m), 938(m), 858(m), 841(m), 813(m), 801(m), 771(s), 748(vs), 682(s), 670(vs), 663(vs), 644(m), 635(m), 621(m), 579(m), 566(m), 380(m), 345(m), 297(m), 258(m), 229(m). Raman (ν /cm⁻¹): 3157(m), 3141(w), 3133(m), 3083(m), 1593(s), 1577(vs), 1500(m), 1354(m), 1347(vs), 1183(m), 1048(vs), 686(vs), 447(s).

Physical Measurements. Vibrational Spectroscopy. IR spectra were recorded as KBr pellets or Nujoll mulls using Perkin-Elmer FTIR-2000 and Perkin-Elmer 1600 spectrophotometers over the frequency range of 4000–50 cm⁻¹. The Raman spectrum of the powder complex was recorded at room temperature on a Jobin-Yvon T6400 spectrometer equipped with a CCD camera and He/Ne laser (λ = 632.8 nm).

UV-vis-NIR Spectroscopy. The absorption (~30% mass of complex in KBr tablet) electronic spectrum was measured on a Cary 500 Scan UV-vis-NIR spectrophotometer. For analysis of the spectra, the variable digital filter method and deconvolution of the spectral contour into Gaussian components¹⁸ were applied.

Magnetic Measurements. Magnetic susceptibility down to 1.9 K at 500 mT and magnetization up to 5 T at 1.9 K were measured with a Quantum Design SQUID magnetometer. Diamagnetic correction (-401×10^{-6} emu mol⁻¹) was calculated using Pascal's constants.

EPR. Low-temperature HF-EPR spectra were recorded at the EMR facility of the NHMFL over the frequency range of 52–432 GHz with magnetic fields up to 14.5 T. Detection was provided by an InSb hot-electron bolometer (QMC Ltd., Cardiff, UK). Magnetic field modulation for detection purposes was employed, and a Stanford SR830 lock-in amplifier converted the modulated signal to a DC voltage. The transmission EPR instrument employed no resonant cavity.

X-ray Structure Determination. Preliminary examination and intensity data collections were carried out on a KUMA KM-4 κ axis diffractometer with graphite-monochromated Mo K α and with scintillation. The data were corrected for Lorentz and polarization effects. The structure was solved by direct methods and refined by the full-matrix least-squares method on all F^2 data using the SHELXTL software.¹⁹ Carbon-bonded hydrogen atoms were included in calculated positions and refined in the riding mode using SHELXTL default parameters. Other hydrogen atoms were located in a difference map and refined freely. All non-hydrogen atoms were refined with anisotropic displacement parameters.

Crystal Data for [Ni(CMA)₂(im)₂(MeOH)₂]. C₃₈H₃₆N₆NiO₈, M = 763.42, triclinic, space group $P\bar{1}$, a = 7.711(5) Å, b = 8.913(5) Å, c = 12.485(5) Å, α = 99.210(5)°, β = 93.480(5)°, γ = 93.980(5)°, V = 842.7(8) Å³, Z = 1, D_{calc} = 1.504 g cm⁻³, T = 100(1) K, $F(000)$ = 398, habit—plate, crystal size 0.7 mm \times 0.4

- (5) Stokvis, E.; Clugston, S. L.; Honek, J. F.; Heck, A. J. R. *J. Protein Chem.* **2000**, *19*, 389.
- (6) Cavet, J. S.; Meng, W.; Pennella, M. A.; Appelhof, R. J.; Gierdoc, D. P.; Robinson, N. J. *J. Biol. Chem.* **2002**, *277*, 38441.
- (7) Odoko, M.; Adachi, Y.; Okabe, N. *Acta Crystallogr., Sect. E* **2002**, *58*, 7.
- (8) Freeman, H. C.; Guss, J. M. *Acta Crystallogr., Sect. B* **1972**, *28*, 2090.
- (9) Sakurai, T.; Iwasaki, H.; Katano, T.; Nakahashi, Y. *Acta Crystallogr., Sect. B* **1978**, *34*, 660.
- (10) Abdael-Rahman, L. H.; Battaglia, L. G.; Sgarabotto, P.; Mahmoud, M. R. *Polyhedron* **1995**, *15*, 1783.
- (11) Drożdżewski, P.; Pawlak, B. *Trans. Met. Chem.* **2003**, *28*, 727.
- (12) Ingot, A. D.; Młochowski, J.; Szulc, Z.; Ingot, O.; Albin, M. *Arch. Immun. Ther. Exp.* **2002**, *33*, 275.
- (13) Miernik, D.; Lis, T.; Palus, J.; Reedijk, J. *Inorg. Chim. Acta* **2002**, *205*, 123.
- (14) Dobrzyńska, D.; Duczmal, M.; Jezierska, J.; Jerzykiewicz, L. B. *Polyhedron* **2002**, *21*, 2381.
- (15) Miernik, D.; Lis, T. *J. Chem. Cryst.* **1994**, *11*, 731.
- (16) Miernik, D.; Lis, T. *Acta Cryst.* **1996**, *C52*, 1171.
- (17) Dobrzyńska, D.; Lis, T. *J. Mol. Struct.* **1997**, *406*, 89.

- (18) (a) Bierman, G.; Ziegler, H. *Anal. Chem.* **1986**, *58*, 536. (b) Myrczek, J. *Spectrosc. Lett.* **1990**, *23*, 1027. (c) Wojciechowska, A.; Staszak, Z.; Pietraszko, A.; Bronowska, W.; Cieślak-Golonka, M. *Polyhedron* **2001**, *21*, 2063. (d) A Slavić, I. *Nucl. Instrum. Methods* **1976**, *134*, 285. (e) Bardecki, A.; Staszak, Z. *Comp. Enh. Spectrosc.* **1984**, *2*, 129. (f) Krzystek, J.; Zvyagin, S. A.; Ozarowski, A.; Trofimenko, S.; Telsler, J. *J. Magn. Reson.* **2006**, *178*, 174. (g) Vongtragool, S.; Gorshunov, B.; Dressel, M.; Krzystek, J.; Eichhorn, D. M.; Telsler, J. *Inorg. Chem.* **2003**, *42*, 1788.
- (19) Sheldrick, G. M. (1998). SHELXTL, Version 5.1.; Bruker AXS Inc.: Madison, WI.

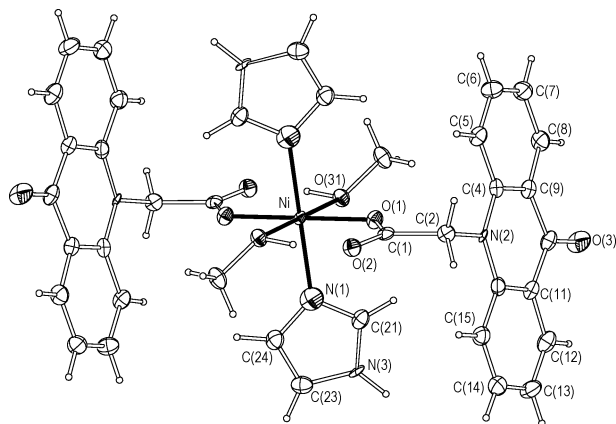


Figure 1. ORTEP drawing of the [Ni(CMA)₂(im)₂(MeOH)₂] molecule. Ellipsoids at 50% probability level are shown.

mm × 0.2 mm, $\mu = 0.642 \text{ mm}^{-1}$, number of reflections measured 3097, number of unique reflections 2922, $R_{\text{int}} = 0.0423$, Θ range 2.32–25.05°, $R_1 [I > 2\sigma(I)]$, 0.0306, 0.1138, $wR_2(\text{all data})$ 0.0345, 0.1169, GOF 1.111.

3. Results and Discussion

Crystal and Molecular Structure. Direct reaction between im, CMAH, and NiCl₂ in methanol solution yields green crystals of the title compound, [Ni(CMA)₂(im)₂(MeOH)₂] (Figure 1). Table 1 presents selected bond lengths and angles. In Table 2, the hydrogen-bonding parameters are collected.

The supramolecular structure of [Ni(CMA)₂(im)₂(MeOH)₂] consists of neutral monomers connected by hydrogen bonds and stacking interactions (Figure 2). The nickel(II) ion, located at the inversion center, is coordinated by two imidazole nitrogen atoms (N(1)), two carboxylate oxygen atoms (O(1)), and two oxygen atoms (O(31)) from methanol molecules. The Ni–O(1) bond length of 2.044(2) Å is shorter than the average (2.100 Å,²⁰ 2.07 Å²¹), characteristic for a carboxylate group coordinated to Ni(II) in monodentate mode. Moreover, the Ni–N(1) distance of 2.067(2) Å is short as compared to that observed for imidazole coordinated to nickel(II).²⁰ The bond length between nickel(II) and methanol oxygen atom is 2.101(2) Å and agrees well with literature data.²⁰ Scheme 2 compares the coordination centers in the Glx1 enzyme³ (a) and in the studied complex (b). The average distance Ni–L, estimated for the single shell of N/O atoms in the enzyme, equals 2.07(2) Å and is identical to the average Ni–L distance found for [Ni(CMA)₂(im)₂(MeOH)₂] (2.069(2) Å).

The geometry of the carboxylate group in the complex differs from that expected for the monodentate mode of carboxylate coordination. The C(1)–O(1) and C(1)–O(2) distances are 1.253(2) and 1.251(2) Å, respectively, and are characteristic of carboxylate bound in both chelate and bridging modes.^{20,22} In our case, the geometry of the carboxylate group is affected by the strong intramolecular

hydrogen bonds. Strong hydrogen bonds between coordinated water molecules and carboxylate oxygen atoms have also been observed in complexes of Co(II)- and Ni(II)-containing imidazole, acetyl-D,L-phenylglycine, and water molecules,¹⁰ where carboxylate groups bind to metal ions in monodentate mode. In the compound studied here, the proximity of the hydroxyl donor group of methanol and the carboxylate oxygen atoms that are coordinated to the nickel(II) ion enables the formation of the three-center hydrogen bonding (Scheme 3).²³ This type of hydrogen bond has been found in amino acids, biological macromolecules, and several metal formates.²⁴ The O(31)–H(31)···O(2), O(1) entity is approximately planar with bond distances and angles similar to those observed in other three-center hydrogen bonds.²⁴

In view of the interactions involving the carboxylate group in [Ni(CMA)₂(im)₂(MeOH)₂], its binding mode can be considered as pseudo-bridging. The geometrical parameters of imidazole correspond to those reported for other complexes,²⁰ where it acts as a neutral ligand. The dihedral angle between the imidazole plane and the equatorial plane of the complex equals 82.60(6)°. The Ni(II) ion is coplanar with both coordinated imidazole molecules. Two acridine rings are parallel to each other, while the imidazole ring is twisted by 55.73(6)° with respect to their plane. Each complex molecule is connected to its neighbors through a strong hydrogen bond in which the imidazole group N(3)–H(3) acts as a donor to the O(3)ⁱⁱ oxygen atom in the CMA[−] ligand. This arrangement results in a 1-D chain structure along the crystallographic *c* axis (Figure 2). Neighboring chains that are connected by π – π bonding between parallel acridine rings (Scheme 4) are related by the symmetry operation $1 - x, 1 - y, 1 - z$.

The π – π interaction in the three-ring acridine system can be described as an offset stacking; however, two rings overlap strictly in the face-to-face fashion. Such extensive aromatic–aromatic contacts are very rare.⁸ Also, three weak interchain C–H···X interactions²⁵ were found (Table 2). The tightly joined molecular chains create a 2-D structure, which is parallel to the *ac*-crystallographic plane.

Vibrational Spectra. Although the vibrational spectra of [Ni(CMA)₂(im)₂(MeOH)₂] are very complicated, some characteristic bands generated by the internal ligand modes can be easily found. Absorptions due to the vibrations of imidazole and of the CMA[−] ion are very close to those found in the spectra of [Cu(CMA)₂(im)₂] \cdot 4H₂O.¹³ The carboxylate group in the studied complex give rise to strong bands located at 1595 and 1389 cm^{−1}. The assignment has been made on the basis of comparison of the IR spectrum of the studied complex to those of other CMA compounds.¹⁷ The value of the $\Delta\nu = \nu_{\text{as}}(\text{COO}) - \nu_{\text{s}}(\text{COO})$ parameter found for the nickel(II) complex (209 cm^{−1}) is smaller by 18 cm^{−1} than that found for the copper(II) complex (227 cm^{−1}).¹³ This observation is in agreement with the structural data as the hydrogen bond between the uncoordinated carboxylate

(20) Orpen, A. G.; Brammer, L.; Allen, F. H.; Kennard, O.; Watson, D. G.; Taylor, R. *J. Chem. Soc., Dalton. Trans.* **1989**, S1.

(21) Hocking, R. K.; Hambley, T. W. *Inorg. Chem.* **2003**, *42*, 2833.

(22) Deacon, G. B.; Phillips, R. J. *Coord. Chem. Rev.* **1980**, *33*, 227.

(23) Jeffrey, G. A. *An Introduction to Hydrogen Bonding*; Oxford University Press: Oxford, 1997.

(24) Glusker, J. P. *Acta Crystallogr., Sect. D* **1995**, *51*, 418.

(25) Desiraju, G. R. *Acc. Chem. Res.* **1991**, *24*, 290.

Table 1. Selected Bond Lengths (Å) and Angles (deg) of [Ni(CMA)₂(im)₂(MeOH)₂]^a

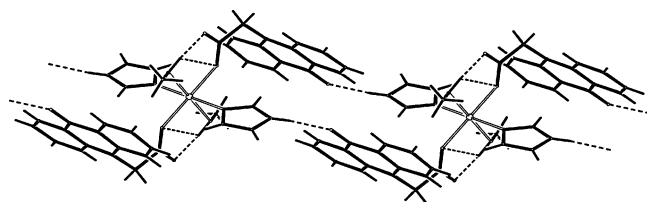
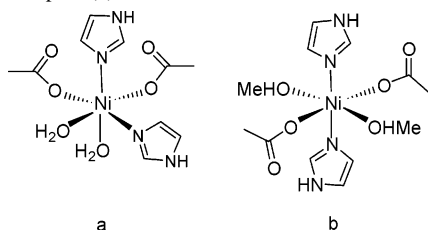
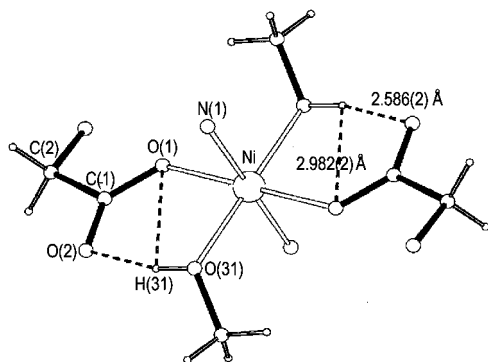
Ni–O(1)	2.044(2)	O(1)–Ni–O(31)	88.02(6)	O(1)–Ni–N(1)	88.79(6)
Ni–O(31)	2.100(2)	O(1)–Ni–O(31) ⁱ	91.98(6)	O(1)–Ni–O(1) ⁱ	91.21(6)
Ni–N(1)	2.067(2)	O(31)–Ni–N(1)	86.17(6)	O(31)–Ni–N(1) ^j	93.83(6)
O(1)–C(1)	1.253(2)	O(1)–C(1)–O(2)	127.0(2)	O(1)–C(1)–C(2)	116.6(1)
O(2)–C(1)	1.251(2)	O(2)–C(1)–C(2)	116.4(1)		

^a Symmetry transformations used to generate equivalent atoms: 1 – x, –y + 1, –z.

Table 2. Hydrogen Bond Parameters for [Ni(CMA)₂(im)₂(MeOH)₂] (Å and deg)^a

D–H···A	d(D–H)	d(H···A)	d(D···A)	<(DHA)
N(3)–H(3N)···O(3) ⁱⁱ	0.88(2)	1.91(2)	2.726(2)	173(2)
O(31)–H(31)···O(2) ^v	0.83(2)	1.72(2)	2.586(2)	167(2)
O(31)–H(31)···O(1) ^v	0.88(2)	2.58(3)	2.980(2)	109(2)
C(12)–H(12)···N(1) ⁱⁱⁱ	0.93(2)	2.96(2)	3.803(3)	151(1)
C(5)–H(5)···O(2) ⁱⁱⁱ	0.93(2)	2.52(2)	3.441(3)	170(1)
C(2)–H(2B)···N(3) ^{iv}	0.97(2)	2.78(2)	3.631(3)	147(1)
C(2)–H(2A)···O(31) ^{iv}	0.93(2)	2.66(2)	3.604(3)	165(1)

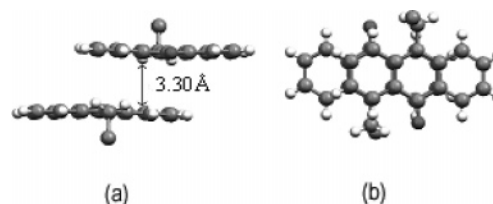
^a Symmetry transformation used to generate equivalent atoms: (ii) –x, –y + 1, –z + 1; (iii) –x + 1, –y + 1, –z; (iv) x + 1, +y, +z; (v) –x, –y + 1, –z.

**Figure 2.** Chain of molecules connected by hydrogen bridges.**Scheme 2.** Comparison of Coordination Centers in Glx1^{3,4} (a) and in the Studied Complex (b)**Scheme 3.** Coordination Sphere of [Ni(CMA)₂(im)₂(MeOH)₂] Showing the D···A Distances in Three-Centered Hydrogen Bonding

oxygen atom and the CMA[–] ligand is significantly stronger in [Ni(CMA)₂(im)₂(MeOH)₂] (A···D distance 2.586(2) Å) than in [Cu(CMA)₂(im)₂]₂·4H₂O (A···D distance 2.830(2) Å).¹³

UV–vis. The UV–vis–NIR electronic spectrum of [Ni(CMA)₂(im)₂(MeOH)₂] (Figure 3) is very similar to the UV–vis spectra of nickel(II) complexes with O, N donors.²⁶

In the diffuse reflectance spectrum of [Ni(CMA)₂(im)₂(MeOH)₂], two different types of bands were observed

Scheme 4. a and b are Mutually Perpendicular Views of π – π Interaction between Acridine Rings Related by Symmetry Operation 1 – x, 1 – y, 1 – z

(Figure 3): (a) in the region 6000–22000 cm^{–1}, two low-intensity bands were attributed to the characteristic spin-allowed and -forbidden transitions of the Ni(II) (d⁸) ion and (b) intense combined bands related to the O, N → Ni(II) and L → L CT transitions appeared in the region of 22000–50000 cm^{–1}.

The crystal structure of the title complex shows that the NiN₂O₂O'₂ chromophore^{10,27} has elongated pseudo-octahedral geometry (Figure 1) and should be analyzed in the local D_{2h} symmetry. Unfortunately, no rhombic splitting of the d–d bands has been observed because the Ni–O(1) (2.044(2) Å) and Ni–N(1) (2.067(2) Å) distances are comparable (Table 1).

The absorption spectrum was adequately analyzed assuming D_{4h} symmetry, where the ground state is the ³B_{1g} (³A₂–(³F)–O_h) term, and six triplet–triplet transitions may be observed.^{26a,28} According to the energy level diagram, the first and second spin-allowed d–d transitions occur between the ³E_g, ³B_{2g} (³T_{2g} (³F)–O_h) and ³A_{2g}, ³E_g (³T_{1g} (³F)–O_h) states, respectively. The first spin-forbidden transition (¹E_g (¹D)–O_h) involves the ¹A_{1g} and ¹B_{1g} states, whereas the second spin-forbidden transition includes only the ¹E_g (¹D) state.²⁸ The filter analysis process revealed a splitting of both d–d bands equal to 2390 cm^{–1} (³E_g and ³B_{2g}) and 2230 cm^{–1} (³A_{2g} and ³E_g). Band analysis was performed with the maximum of four Gaussian curves corresponding to the two components of both d–d bands. Part of the low-energy branch of the ³E_g

- (26) (a) Maslejova, A.; Boča, R.; Dlhán, L.; Papánková, B.; Svoboda, I.; Fuess, H. *Chem. Phys. Lett.* **2001**, *347*, 397. (b) Ihara, Y.; Shinmura, K.; Shibuya, K.; Imai, H.; Sone, K. *Thermochim. Acta* **1995**, *254*, 219. (c) Martin, L. Y.; Sperati, C. R.; Busch, D. H. *J. Am. Chem. Soc.* **1977**, *99*, 2968. (d) Fan, J.; Zhang, Y.; Okamura, T.; Zou, Z.; Ueyama, N.; Sun, W. *Inorg. Chem. Comm.* **2001**, *4*, 501.
- (27) (a) Bunel, S.; Gil, L.; Moraga, E.; Bobadilla, H. *Inorg. Chim. Acta* **1970**, *4*, 415. (b) Orihuela, S.; Sanchez, M. P.; Quiros, M.; Martin, D.; Faure, R. *Polyhedron* **1998**, *17*, 2477. (c) Barea, E.; Navarro, J. A. R.; Salas, J. M.; Masciocchi, N.; Galli, S.; Sironi, A. *Inorg. Chem.* **2004**, *43*, 473. (d) Bronowska, W.; Staszak, Z.; Daszkiewicz, M.; Cieślak-Golonka, M.; Wojciechowska, A. *Polyhedron* **2002**, *21*, 997.
- (28) (a) Lever, A. B. P. *Inorganic Electronic Spectroscopy*; Elsevier: New York, 1984. (b) Perumareddi, J. R. *J. Phys. Chem.* **1972**, *76*, 3401. (c) Merriam, J. S.; Perumareddi, J. R. *J. Phys. Chem.* **1975**, *79*, 142. (d) Vermaas, A.; Groeneveld, W. L.; Reedijk, J. *Z. Naturforsch., A: Phys. Sci.* **1977**, *32*, 632. (e) Rowley, D. A.; Drago, R. S. *Inorg. Chem.* **1967**, *6*, 1092; *Ibid.*, **1968**, *7*, 795.

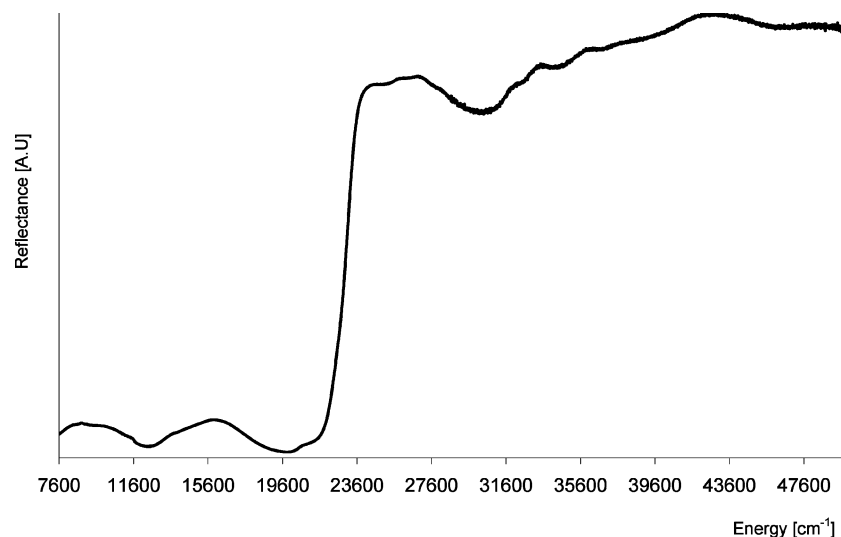


Figure 3. Diffuse-reflectance spectrum of the title complex.

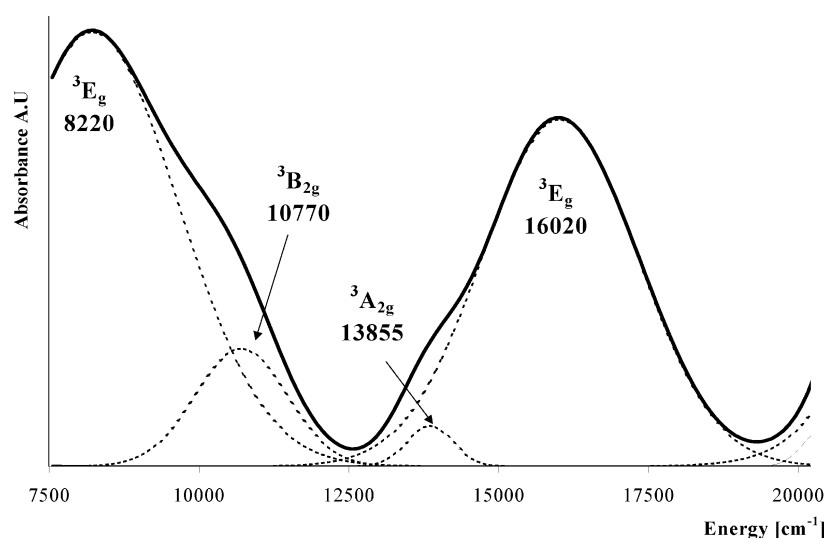


Figure 4. Electronic spectrum of the title complex deconvoluted into Gaussian components.

component was obscured by the noise. We cannot observe the third d–d band assigned as ${}^3P \rightarrow {}^3F$ transition (which consists of ${}^3A_{2g}$ and 3E_g (${}^3T_{1g}({}^3P) - O_h$) components in D_{4h} symmetry) and the second spin-forbidden transition ${}^1E_g({}^1D)$ because these bands have been obscured by CT transitions originating from imidazole ring orbitals $\pi_{1,2}(\text{imidazole}) \rightarrow \sigma^* - \text{Ni}$,²⁹ which appear as a broadband at ca. 25 000 cm^{-1} . The Gaussian analysis has not included the bands assigned as the spin-forbidden transitions ${}^3B_{1g} \rightarrow {}^1A_{1g}$ and ${}^1B_{1g}$. These absorptions may exhibit misleading intensities because of their overlap or interaction with a stronger spin-allowed transition. The calculated energies for the spin-forbidden transitions are ca. 12 900 cm^{-1} for ${}^1A_{1g}$, ${}^1B_{1g}$, 22 000 cm^{-1} for ${}^1E_g({}^1D)$, and ca. 24 700 cm^{-1} for ${}^1B_{2g}({}^1D)$, ${}^1A_{1g}({}^1G)$. Results of the best-fit Gaussian analysis are presented in Figure 4.

The energies of the 3E_g , ${}^3B_{2g}$, ${}^3A_{2g}$, and 3E_g states were used in evaluation of the crystal-field parameters (in cm^{-1}): $Dq = 1077$, Racah $B = 930$ ($C = 4B$), $Dt = 257$, and Ds

$= 735$, which are reasonable and acceptable. The B values found for the NiN_2O_4 polyhedron in the title compound are comparable to those for Ni(II) complexes described previously.^{26a,27d,28b–d,30} The positive value of the Dt parameter indicates that the strength of the in-plane ligand field is greater than the axial ligand field.

High-Field and High-Frequency EPR. The HF-HFEPER spectra of the title compound were of very poor quality due to broad lines and magnetic torquing. The latter effect results in a shape of an EPR spectrum far from that expected for random distribution of molecules, thus making EPR simulations unreliable. Such effects are often encountered in high-field EPR, but this case was exceptionally difficult. Figure 5a shows a spectrum of loose powder recorded at 30 K and 203.2 GHz, which has a striking aspect of a single-crystal spectrum in that the crystallites are largely oriented with their Y axes parallel to the field. Pressing the powder into a pellet resulted in very dramatic change of the spectral shape (Figure 5).

(29) Bernarducci, E.; Schwindinger, W. F.; Hughey, J. L.; Krogh-Jespersen, K.; Schugar, H. J. *J. Am. Chem. Soc.* **1981**, *103*, 1686.

(30) Pietraszko, A.; Bronowska, W.; Wojciechowska, A.; Staszak, Z.; Cieślak-Golonka, M. *Pol. J. Chem.* **2002**, *76*, 151.

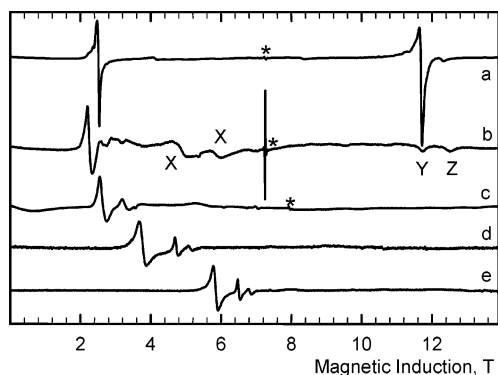


Figure 5. EPR spectra at 30 K: (a) loose powder, 203.2 GHz and (b–e) compressed pellet: (b) 203.2 GHz; (c) 222.4 GHz; (d) 324.0 GHz, and (e) 432.0 GHz. Asterisks indicate signals of the DPPH standard ($g = 2.0037$). An approximate zero-field transition is seen in trace c.

We also tried pressing pellets of the complex mixed with KBr, but despite all our efforts, we never obtained a correct powder EPR pattern. Two zero-field transitions were fortunately observed at ca. 222 GHz (Figure 5) and at ca. 98 GHz, allowing us to estimate the D and E parameters of the spin Hamiltonian

$$H = \mu_B B g S + D[S_z^2 - 1/3S(S+1)] + E(S_x^2 - S_y^2) \quad (1)$$

In a spin-triplet spectrum, three zero-field transitions are possible, and they appear at microwave frequencies $2E$, $D - E$, and $D + E$, respectively. In our case, the third transition must appear at either the sum or the difference of the frequencies above, for example, ~ 124 GHz or ~ 320 GHz. We do not have a microwave source available for the 112–184 GHz range; thus, we cannot directly check the first possibility. We do not observe a zero-field transition in the 288–336 GHz range that is covered by our source. Thus, we can label the 98 and 222 GHz transitions as $2E$ and $D + E$, respectively, resulting in $D = 173$ GHz (5.8 cm^{-1}) and $E = 49$ GHz (1.6 cm^{-1}). The D and E values as well as the g components were subsequently refined by fitting the frequency dependencies of the signal position (Figure 6).

Magnetic Properties. The magnetic susceptibility (Figure 7) shows Curie–Weiss behavior in the temperature range of 150–300 K with the moment $\mu = 3.19\mu_B$ and the Weiss constant $\theta = -7.5$ K. The susceptibility was fitted to eq 2 over the entire temperature range of 1.9–300 K using exact energies E_i and eigenvectors of the three sublevels of the $S = 1$ state resulting from full matrix diagonalization of the spin Hamiltonian (eq 1)

$$\chi = -\frac{Ng \sum_{i=1}^3 \sum_{j=1}^3 |c_{ij}|^2 M_j \exp(-E_i/kT)}{B \sum_{i=1}^3 \exp(-E_i/kT)} + N\alpha \quad (2)$$

where c_{ij} are the coefficients of the M_S states $|-1\rangle$, $|0\rangle$, and $|1\rangle$ in eigenvector i . Powder susceptibilities were taken as the average of values calculated at the molecular orientations X , Y , and Z .

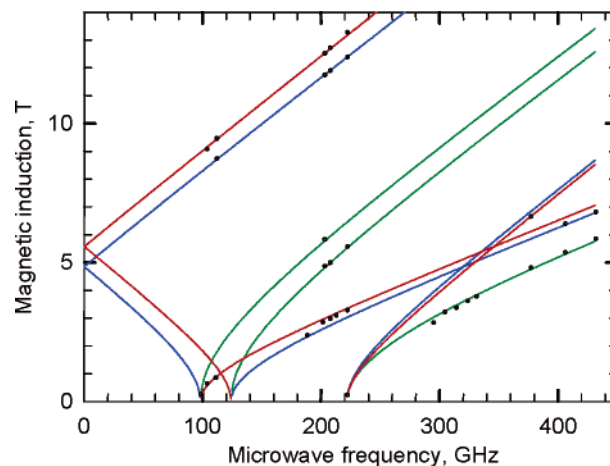


Figure 6. Frequency dependencies of the turning points corresponding to the canonical orientations of molecules vs the magnetic field. Green, blue, and red lines are calculated for the magnetic field parallel to the molecular axes X , Y , and Z , respectively, with the following parameters: $g_x = 2.29(1)$, $g_y = 2.18(1)$, $g_z = 2.13(1)$, $D = 5.77(1)$ cm^{-1} , and $E = 1.636(2)$ cm^{-1} .

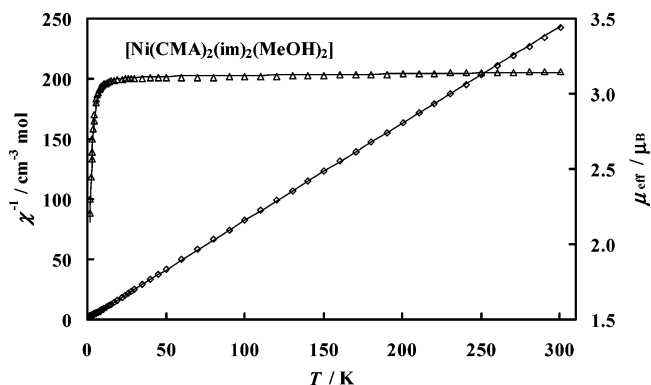


Figure 7. Reciprocal magnetic susceptibility (diamonds) and effective moment (triangles). The solid line was calculated with $D = 5.77$ cm^{-1} , $E = 1.636$ cm^{-1} , $g_x = 2.29(1)$, $g_y = 2.18(1)$, $g_z = 2.13(1)$, and $N\alpha = 75 \times 10^{-6}$ cgs emu (TIP).

Assuming the D , E , and g_x , g_y , g_z parameters determined from the EPR measurements, we found the temperature-independent paramagnetism (TIP) $N\alpha = 75 \times 10^{-6}$ cm^3/mol (the agreement factor $R = \sum[(\chi T)_{\text{exp}} - (\chi T)_{\text{calc}}]^2 / \sum[(\chi T)_{\text{exp}}]^2 = 1.5 \times 10^{-4}$). The result is shown in Figure 7 as solid lines. Figure 8 shows the field dependence of magnetization at 1.9 K. The solid line is the theoretical curve calculated with the ZFS and $N\alpha$ parameters applied earlier to the fitting of the susceptibility versus temperature curve. The agreement of the calculated and experimental magnetization is good, which confirms the consistency of the analysis of all magnetic data. It is noteworthy that a better magnetization fit may be obtained with a negative D value (-5.77 cm^{-1}). However, the analysis of electronic spectra with full configuration interactions and spin–orbit coupling included definitely yielded the ground level $^3B_{1g}$ split into a lower Γ_4 singlet and a higher lying Γ_5 doublet.³¹ The $\Gamma_5 - \Gamma_4$ gap corresponds to the ZFS D parameter.³² Assuming the effective single-electron spin–orbit coupling parameter ζ for Ni(II) equal to 550 cm^{-1} , the energy difference of 5.9 cm^{-1} was obtained, not far from the EPR D value.

(31) J. Telsler, personal communication.

(32) Boča, R. *Struct. Bonding (Berlin)* **2006**, *117*, 1.

Table 3. Single-Ion ZFS Parameters for Ni(II) Complexes with Distorted Tetragonal Bipyramidal Coordination^a

complex	<i>D</i> (cm ⁻¹)	<i>E</i> (cm ⁻¹)	coordination	ref	method ^b
[Ni(CMA) ₂ (im) ₂ (MeOH) ₂]	+5.6	1.8	<i>trans</i> -NiO ₄ N ₂	this paper	
[Ni(Him2-py) ₂ NO ₃]NO ₃	-10.15	0.1	<i>cis</i> -NiO ₂ N ₄	39	b-d
[Ni(dmiz) ₂ (ac) ₂]	-9.94		<i>trans</i> -NiO ₂ N ₄	36	a and b
NiCl ₂ ·4H ₂ O	-7.99		<i>cis</i> -NiCl ₂ O ₄	40	a and e
[Ni(terpy) ₂](PF ₆) ₂	-6.10	0.12	<i>trans</i> -NiN ₄ N' ₂	41	a and b
[Ni _{0.09} Zn _{3.91} (hmp) ₂ (dmb) ₄ Cl ₄]	-5.30	1.20	<i>cis</i> -NiClO ₄ N	42	c
[Ni _{0.07} Zn _{0.93} (ox)(dmiz) ₂]	+1.875	0.38	<i>cis</i> -NiO ₄ N ₂	37	c
[Ni(EtL) ₂ (Me ₅ dien)]	+2.98	0.69	<i>trans</i> -NiO ₂ N ₄	43	c
[ReCl ₄ (<i>m</i> -ox)Ni(dmphen) ₂]·CH ₃ CN	6.1		<i>cis</i> -NiO ₂ N ₄	44	a
[Ni(L _{NNOO}) ₂ (H ₂ O) ₂]	+9.47	1.54	<i>trans</i> -NiO ₄ N ₂	45	a
[Ni ₄ (MeOH) ₄ (sal-2-en) ₄]	+13		NiO ₅ N	46	a, d, and f

^a Abbreviations: ac = acetato(1-); dmb = 3,3-dimethyl-1-butanol; dmiz = dimethylimidazole; dmphen = 2,9-dimethyl-1,10-phenantroline; EtL = 2-oxypropiofenone oxime(1-); Him2-py = 2-(2'-pyridyl)-4,4,5,5-tetramethyl-4,5-dihydro-1H-imidazolyl-1-hydroxy; hmp = 2-hydroxymethylpyridine(1-); L_{NNOO} = C(CN)₂NO·MeOH; Me₅dien = pentamethyldiethylenetriamine; ox = oxalato(2-); sal-2-en = salicylidene-2-ethanolamine; and terpy = 2,2',6'2'-terpyridine. ^b Experimental methods: (a) temperature dependence of susceptibility; (b) field dependence of magnetization; (c) high-field and high-frequency EPR (HF-HFEPR); (d) frequency domain magnetic resonance spectroscopy (FDMRS); (e) specific heat; and (f) inelastic neutron scattering (INS).

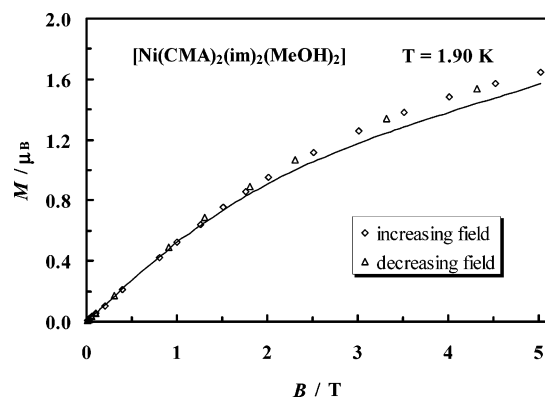


Figure 8. Magnetization as a function of magnetic induction at 1.9 K. The solid line was calculated with the same parameters as the susceptibility (Figure 7).

The ZFS parameters of transition metal ions attract considerable attention. Large negative axial parameter *D* is necessary for a compound to act as a single-molecule magnet.³³ A comprehensive review of ZFS parameters in metal complexes, with special emphasis put on the Ni(II) compounds, was recently published.^{34,35} It has been shown that *D* varies between -22 and +9.5 cm⁻¹ for distorted octahedral (coordination number 6) mono- and polynuclear Ni(II) complexes. It is difficult to notice a clear *D* dependence on atoms in the first coordination sphere, but its value grows markedly with increasing distortion of the coordination polyhedron.³⁶ Ni(II) complexes with distorted tetragonal bipyramidal coordination exhibit relatively high values of *D* (Table 3). The noticeable exception in Table 3 is the chain antiferromagnet [Ni(C₂O₄)(dmiz)₂],³⁷ with a small *D* value. The origin of this phenomenon is not clear because the coordination sphere of nickel ion is highly distorted (*cis*-NiN₂O₄ coordination), but it is worth noting that ZFS splitting in chain compounds is usually small.³⁸

(33) Gatteschi, D.; Sessoli, R. *Angew. Chem., Int. Ed.* **2003**, *42*, 268.

(34) Boča, R. *Coord. Chem. Rev.* **2004**, *248*, 757.

(35) Krzystek, J.; Ozarowski, A.; Telsler, J. *Coord. Chem. Rev.* **2006**, *250*, 2308.

(36) Boča, R.; Dlhád, L.; Haase, W.; Herchel, R.; Mašlejová, A.; Papánková, B. *Chem. Phys. Lett.* **2003**, *373*, 402.

(37) Pardi, L. A.; Hassan, A. K.; Hulsbergen, F. B.; Reedijk, J.; Spek, A. L.; Brunel, L.-C. *Inorg. Chem.* **2000**, *39*, 159.

4. Conclusion

In summary, we prepared and characterized a mixed ligand complex in which the coordination environment of nickel is very similar to the active site found in the GlxI enzyme. The structural parameters found for the nickel environment in the enzyme and in the studied complex are very close. Very strong intramolecular hydrogen bonds shape the geometry of the carboxylate group and affect its infrared spectrum. The intermolecular hydrogen bonds create chains of molecules. Further, strong overlapping of the acridine rings of neighboring chains cause them to arrange into 2-D structures. The electronic spectroscopy data are successfully correlated with crystallographic and magnetic results. The electronic absorption shape is consistent with the NiN₂O₂O'₂ chromophore. Assignment of the electronic bands to the respective transition in *D*_{4h} symmetry, based on the Gaussian analysis, allowed the determination of the crystal field parameter, *Dq*, and of the Racah parameter, *B*. The ZFS parameters of the Ni(II) ions determined from the multiple frequency high-field EPR measurements were successfully applied to calculate the magnetic susceptibility and magnetization. The detailed spectroscopic and magnetic studies performed in this work have provided reliable experimental

(38) (a) Boča, R.; Boča, M.; Gembický, M.; Jäger, L.; Wagner, C.; Fuess, H. *Polyhedron* **2004**, *23*, 2337. (b) Żurowska, B.; Mroziński, J.; Julve, M.; Lloret, F.; Mašlejová, A.; Sawka-Dobrowolska, W. *Inorg. Chem.* **2002**, *41*, 1771. (c) Černák, J.; Abboud, K. A.; Chomič, J.; Meisel, M. W.; Orendáč, M.; Orendáčová, A.; Feher, A. *Inorg. Chim. Acta* **2000**, *311*, 126.

(39) Rogez, G.; Rebilly, J.-N.; Barra, A.-L.; Sorace, L.; Blondin, G.; Kirchner, N.; Duran, M.; van Slageren, J.; Parsons, S.; Ricard, L.; Marvilliers, A.; Mallah, T. *Angew. Chem., Int. Ed.* **2005**, *44*, 1876.

(40) McElearney, J. N.; Losee, D. B.; Merchant, S.; Carlin, R. L. *Phys. Rev.* **1973**, *B7*, 3314.

(41) Waldman, O.; Hassmann, J.; Müller, P.; Volkmer, D.; Schubert, U. S.; Lehn, J.-M. *Phys. Rev. B* **1998**, *58*, 3277.

(42) Yang, E.-C.; Kirman, C.; Lawrence, J.; Zakharov, L. N.; Rheingold, A. R.; Hill, S.; Henrickson, D. N. *Inorg. Chem.* **2005**, *44*, 3827.

(43) Collison, D.; Helliwell, M.; Jones, V. M.; Mabbs, F. E.; McInnes, E. J. L.; Riedi, P. C.; Smith, G. M.; Pritchard, R. G.; Cross, W. I. *J. Chem. Soc., Faraday Trans.* **1998**, *94*, 3019.

(44) Chiozzzone, R.; González, R.; Kremer, C.; De Munno, G.; Armentano, D.; Lloret, F.; Julve, M.; Faus, J. *Inorg. Chem.* **2003**, *42*, 1064.

(45) Boča, R.; Baran, P.; Dlhád, L.; Hvastijová, M.; Wltschek, G. *Chem. Phys. Lett.* **1998**, *284*, 254.

(46) Sieber, A.; Boskovic, C.; Bircher, R.; Waldmann, O.; Ochsenbein, S. T.; Chaboussant, G.; Gudel, H. U.; Kirchner, N.; van Slageren, J.; Wernsdorfer, W.; Neels, A.; Stoeckli-Evans, H.; Janssen, S.; Juranyi, F.; Mutka, H. *Inorg. Chem.* **2005**, *44*, 4315.

data for determination of the electronic structure of the metal enzyme center. These results are indispensable for the proper description of the enzyme activity. This work contributes to the characterization of NiGlx1 models and is therefore relevant to nickel biochemistry.

Acknowledgment. We thank Dr. J. Telser from Roosevelt University for fruitful discussions. This work was supported by the Wrocław University of Technology Project W3 343509), by the National High Magnetic Field Laboratory,

which is funded by the NSF through Cooperative Agreement DMR 0084173, and by the State of Florida.

Supporting Information Available: Supplementary data on [Ni(CMA)₂(im)₂(MeOH)₂] from CCDC— (e-mail: deposit@ccdc.cam.ac.uk or <http://www.ccdc.cam.ac.uk>) upon request, quoting deposition number 242969. This material is available free of charge via the Internet at <http://pubs.acs.org>.

IC060886T